Quantifying the Native Energetics Stabilizing Bacteriorhodopsin by Single-Molecule Force Spectroscopy

Hao Yu,[1,†] David R. Jacobson,[2,†] Hao Luo,[1] and Thomas T. Perkins[2,3,*]
[1]School of Physics, Huazhong University of Science and Technology, Wuhan 430074, China
[2]JILA, National Institute of Standards and Technology and University of Colorado, Boulder, Colorado 80309, USA
[3]Department of Molecular, Cellular, and Developmental Biology, University of Colorado, Boulder, Colorado 80309, USA

(Received 10 April 2020; accepted 2 July 2020; published 5 August 2020)

We quantified the equilibrium (un)folding free energy ΔG_0 of an eight-amino-acid region starting from the fully folded state of the model membrane-protein bacteriorhodopsin using single-molecule force spectroscopy. Analysis of equilibrium and nonequilibrium data yielded consistent, high-precision determinations of ΔG_0 via multiple techniques (force-dependent kinetics, Crooks fluctuation theorem, and inverse Boltzmann analysis). We also deduced the full 1D projection of the free-energy landscape in this region. Importantly, ΔG_0 was determined in bacteriorhodopsin's native bilayer, an advance over traditional results obtained by chemical denaturation in nonphysiological detergent micelles.

DOI: 10.1103/PhysRevLett.125.068102

Precise quantification of membrane-protein folding energetics is a long-sought goal. While membrane proteins fold *in vivo* via the translocon [1], the final folded state is believed to be at thermodynamic equilibrium [1–3]. Thus, *in vitro* measurements of the free energy of unfolding ΔG_0 give insight into the balance of interactions stabilizing the folded structure (e.g., van der Waals, hydrophobicity, hydrogen bonding) [4]. ΔG_0 for globally unfolding membrane proteins is typically determined by chemical denaturation using sodium dodecyl sulfate [5–11]. ΔG_0 for the model membrane-protein bacteriorhodopsin (BR) is particularly well characterized [6,12–17]. However, four notable limitations of these chemical-denaturation measurements are (i) the measurements are made in a nonnative lipid environment; (ii) they involve extrapolation from high denaturant concentration to zero [18]; (iii) the denatured "unfolded" state is ill-defined and retains ~60% of its native-state α-helical secondary structure [Fig. 1(a), inset] [19–21]; and (iv) the requirement of reversible unfolding and refolding excludes the vast majority of proteins, including *G*-protein coupled receptors [22]. These limitations motivate the development of alternate techniques with different underlying assumptions, including steric trapping [18] and magnetic-tweezers-based [23] assays. In this Letter, we demonstrate an approach based on local unfolding and refolding of BR in its native bilayer by atomic-force microscopy (AFM).

Force-induced unfolding of BR by AFM overcomes many limitations of chemical-denaturation experiments [Fig. 1(a)] [24–26]. In particular, measurements can be made in the native bilayer (i.e., purple membrane), preserving native protein-lipid and protein-protein interactions. Moreover, mechanical denaturation leads to a well-defined, fully stretched unfolded state. Finally, local unfolding of a small region of the protein means that unfolding need not be globally reversible and that tertiary interactions with the rest of the protein are maintained. Notwithstanding these advantages, prior AFM measurements of ΔG_0 [27–29] have had their own limitations. Prior studies measured ΔG_0 for removing the final five of BR's seven transmembrane helices and were therefore insensitive to the full set of tertiary interactions present in the fully folded structure. These AFM measurements were also performed far from equilibrium, making it difficult to recover equilibrium thermodynamic quantities [30]. Finally, earlier studies did not account for the work of stretching the unfolded polypeptide, adding an anomalous contribution to ΔG_0.

To overcome these limitations, we required an AFM with sufficient spatiotemporal resolution to detect rapid unfolding and refolding transitions and an assay that could repeatedly unfold and refold individual molecules over many seconds. We achieved this by incorporating recent advancements in AFM-based force spectroscopy into the assay depicted in Fig. 1(a). In this assay, the AFM cantilever exerts force on the *C*-terminal tail of BR, causing it to unfold in a series of steps, each corresponding to a metastable unfolding intermediate [24,31]. We used ultrashort cantilevers ($L = 9$ μm) modified with a focused ion beam [32–34] to have ~2-μs resolution, ~10–25 pN/nm stiffness, and sub-pN force stability over ~5–10 s (see Fig. S1 in the Supplemental Material [35]). To allow precise unfolding of the first helix pair over long timescales and with reduced nonspecific adhesion, we used copper-free click chemistry to establish *in situ*, site-specific covalent coupling of the AFM tip to BR (see Supplemental Material) [32,35,39].

BR unfolding satisfied the biophysical requirements of these measurements because BR undergoes rapid reversible

 © 2020 American Physical Society

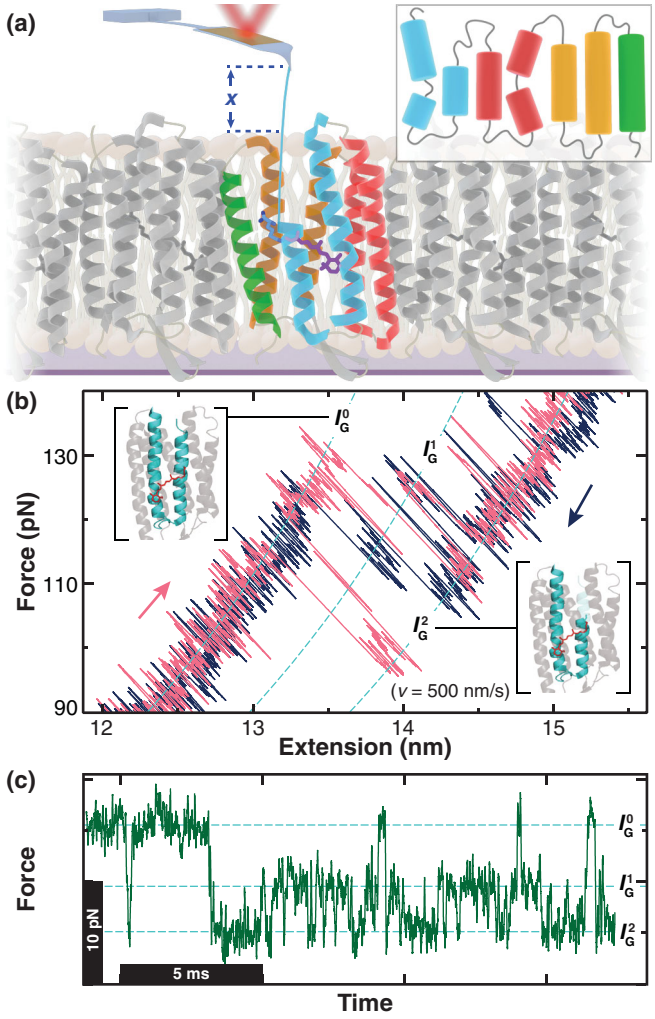

FIG. 1. Probing the energetics of bacteriorhodopsin (BR) starting from its fully folded state. (a) In this AFM assay, BR embedded in native membrane is unfolded from its C-terminal tail into a well-defined, fully stretched state with extension x. Inset: sketch of the unfolded state in a traditional chemical-denaturation experiment. Note, ~60% of native α-helical secondary structure remains. (b) Reversible nonequilibrium force-extension curves span three structural states, separated by five and three amino acids, respectively. The graph shows one cycle of cantilever retraction (pink) and approach (blue). Segments corresponding to individual states were well fit by an elastic model (dashed lines). Insets: structures of two of the states. (c) Force- vs time record shows equilibrium transitions between the same three states (dashed lines). Data smoothed to 17 kHz.

transitions between three states—termed I_G^0, I_G^1, and I_G^2—spanning eight amino acids during initial unfolding from its fully folded state. Local unfolding while the rest of the protein remains folded enables access to the underlying energetics including intact native tertiary interactions. These three states were probed over multiple seconds without full unfolding because I_G^2 is mechanically stabilized by the retinal cofactor [32]. Two AFM data-acquisition protocols were used to acquire nonequilibrium and equilibrium data on single molecules [40]. In the nonequilibrium protocol, the cantilever was alternatingly retracted from and moved toward the surface, inducing unfolding and refolding. For each molecule, we obtained 38–65 unfolding and refolding cycles over three pulling velocities ($v = 200$, 300, and 500 nm/s). A partial example cycle is shown in Fig. 1(b), where near-equilibrium transitions occurred between three states; each state was well modeled by a wormlike chain (WLC) [41,42] in series with a PEG linker [43]. In the equilibrium protocol, the position of the cantilever base was fixed and the protein repeatedly transitioned between states [Fig. 1(c)] [40,44]. Both protocols could be applied sequentially to the same molecule, leading to $\sim 10^4$ detected transitions per molecule over ~10 s. From these data, we determined ΔG_0 for this eight-amino-acid region via three methods: force-dependent transition kinetics [45], the Crooks fluctuation theorem [46], and inverse-Boltzmann analysis [45].

In the first of these methods, we analyzed nonequilibrium trajectories of unfolding and refolding to obtain the force-dependent transition rates between states i and j, $k_{ij}(F)$, which encode properties of the underlying equilibrium free-energy landscape. Transition rates are a valuable approach to analyzing multistate force-spectroscopy data because they are not biased by sequential transitions that occur at similar forces [47], in contrast to analyses of rupture-force distributions. We calculated $k_{ij}(F)$ based upon the method of Zhang and Dudko, which involves counting transitions in force bins [47]. To do so, we smoothed the data to 35–90 kHz to obtain an acceptable signal-to-noise ratio for resolving transitions [Fig. 2(a)], and then identified transitions using a hidden-Markov model [48]. Technical details of this and other analyses are presented in the Supplemental Material [35].

We computed the force-dependent kinetics in two steps. We first divided the force domain into 10-pN bins and, for each bin, determined the number of transitions from state i to state j, $N_{ij}(F)$, and the amount of time spent occupying state i, $t_i(F)$. We found initial force-dependent rate constants by evaluating

$$k_{ij}(F) = \frac{N_{ij}(F)}{t_i(F)}. \tag{1}$$

We used this formula [49], rather than that proposed by Zhang and Dudko [47], to avoid dividing by zero for sparsely occupied states. Second, we corrected this initial rate map for the effective instrument time resolution of $\tau = 13$–29 μs, including the effect of smoothing. This correction, detailed and verified by simulations in an accompanying paper [50], was based on the Poisson statistics of barrier-crossing transitions and allowed rates to be calculated even when of order $1/\tau$. The corrected rate map is shown in Fig. 2(b).

To determine ΔG_0 for each transition, we next obtained $F_{1/2}$, the force of equal unfolding and refolding rates, from

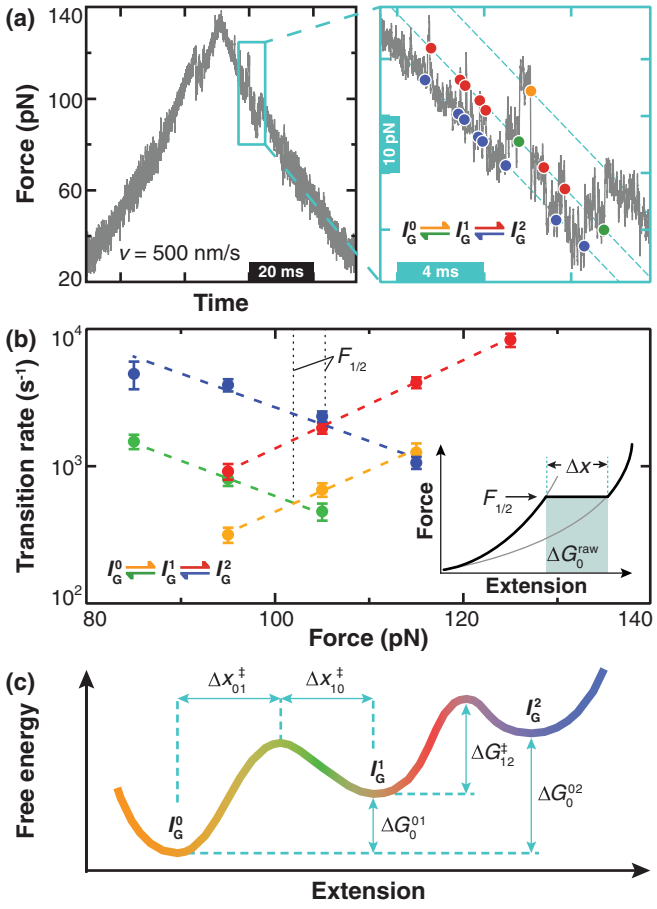

FIG. 2. ΔG_0 determined from transition kinetics of nonequilibrium data. (a) Left: example unfolding and refolding cycle. A typical single-molecule record has ~40–60 such cycles. Right: enlargement showing individual transitions (colored circles). (b) Force-dependent rates for all four transitions. Error bars are standard errors of the mean from a bootstrap analysis. Lines are Bell-model fits. Line crossings reveal $F_{1/2}$, the equilibrium unfolding force. Inset: illustration of how the uncorrected unfolding free energy was obtained as $\Delta G_0^{\mathrm{raw}} = F_{1/2}\,\Delta x$, which was then corrected for work done to stretch the unfolded section of the protein. (c) Scheme of the underlying free-energy landscape. ΔG_0 denotes a change in free energy between stable states, $\Delta G^{\ddagger}$ is the height of a transition barrier, and $\Delta x^{\ddagger}$ is the distance from a stable state to that barrier.

the intersection of Bell-model fits [51] to the rate maps. These fits also yielded two energy-landscape parameters: the zero-force rate constant k_0 and the distance to the transition state $\Delta x^{\ddagger}$ [Fig. 2(c)]. Unfortunately, we could not use a more sophisticated model [52] to additionally constrain the height of the transition barrier $\Delta G^{\ddagger}$ because curvature was not observed in $\log(k)$ vs F.

Finally, we determined ΔG_0 between states by multiplying $F_{1/2}$ by the unfolding extension change and then correcting for the work to stretch the newly unfolded segment [45,53]. Because $F_{1/2}$ is the unfolding force in the constant-force ensemble, the equilibrium work done on the system at unfolding is simply this force times the unfolding extension change at $F_{1/2}$ [45,53,54]. The resulting work included both the work done to unfold the protein and that done to stretch the newly unfolded portion of the protein to $F_{1/2}$. Unlike prior membrane-protein studies, we subtracted the latter correction—here an 18% effect—to yield the free-energy change associated specifically with unfolding the protein:

$$\Delta G_0 = F_{1/2}(\Delta x - \Delta d) - \int_{\Delta d}^{\Delta x} F_{\mathrm{WLC}}(x')dx', \qquad (2)$$

where Δx is the extension of the unfolded region and Δd is the nonzero extension of that region along the pulling axis before unfolding [44,55] (see Supplemental Material, Fig. S2 [35]). We obtained Δd from the crystal structure of BR [56], an approach that could introduce an error for less-constrained proteins (e.g., significantly unfolded or in non-native membrane). Evaluating Eq. (2) for each of ten molecules (18 541 total transitions), we obtained $\Delta G_0^{01} = 18.2 \pm 0.7\,k_BT$ (mean ± SEM) for the first transition and $\Delta G_0^{12} = 9.5 \pm 0.4\,k_BT$ for the second, totaling to $\Delta G_0^{02} = 27.7 \pm 0.8\,k_BT$.

In the second nonequilibrium data analysis, we applied the Crooks fluctuation theorem (CFT) to calculate equilibrium ΔG_0 from the nonequilibrium work W_{raw} done to drive unfolding or refolding [46,57]. This work is the area under the curve of F versus cantilever height Z [Fig. 3(a)] and includes the work done on the protein W, as well as the work done to deflect the cantilever and to stretch the unfolded polypeptide chain. The latter contributions were subtracted to give the work done on the folded protein:

$$W = W_{\mathrm{raw}} - \Delta G_{\mathrm{cant}} - \Delta G_{\mathrm{linker}} - \Delta G_{\mathrm{released}}, \qquad (3)$$

where ΔG_{cant} is the work done on the cantilever (modeled as a linear spring), $\Delta G_{\mathrm{linker}}$ is the work done on the C-terminal polypeptide tail (modeled as a WLC) and PEG linker (modeled following Oesterhelt *et al.* [43]), and $\Delta G_{\mathrm{released}}$ is the work done to stretch the eight-amino-acid region upon unfolding (terms defined in Supplemental Material [35]). These corrections may be made either before or after applying the CFT because they depend only on the limits of the integration. ΔG_0 was calculated using

$$\frac{P_U(W)}{P_R(-W)} = \exp\left(\frac{W - \Delta G_0}{k_BT}\right), \qquad (4)$$

where $P_U(W)$ and $P_R(-W)$ are the histograms of works during unfolding and refolding, respectively [46]. Equation (4) implies that $\Delta G_0 = W$ where the two histograms cross. This analysis is shown for the $v = 500$ nm/s data of one representative molecule in Fig. 3(b). Because the histogram widths were large compared with their

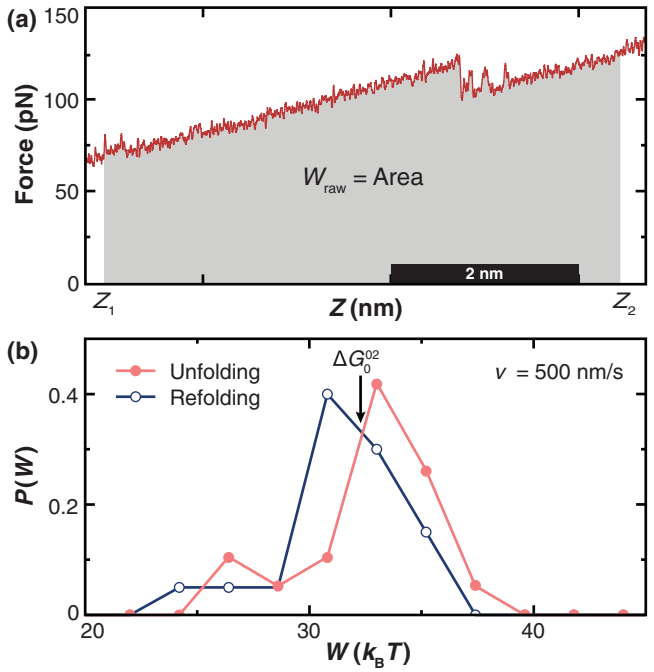

FIG. 3. Determining ΔG_0^{02} from the Crooks fluctuation theorem. (a) Integrating $F(Z)$ (gray) yielded the raw work W_{raw} done on the entire experimental system, where Z is the position of the cantilever base. (b) Histograms of work W done on a particular individual protein as it was repeatedly unfolded (red, closed) and refolded (blue, open) 20 times at $v = 500$ nm/s. W was obtained from W_{raw} by subtracting the work done on the cantilever and polypeptide chain [Eq. (3)]. ΔG_0 is the crossing point of the distributions (arrow).

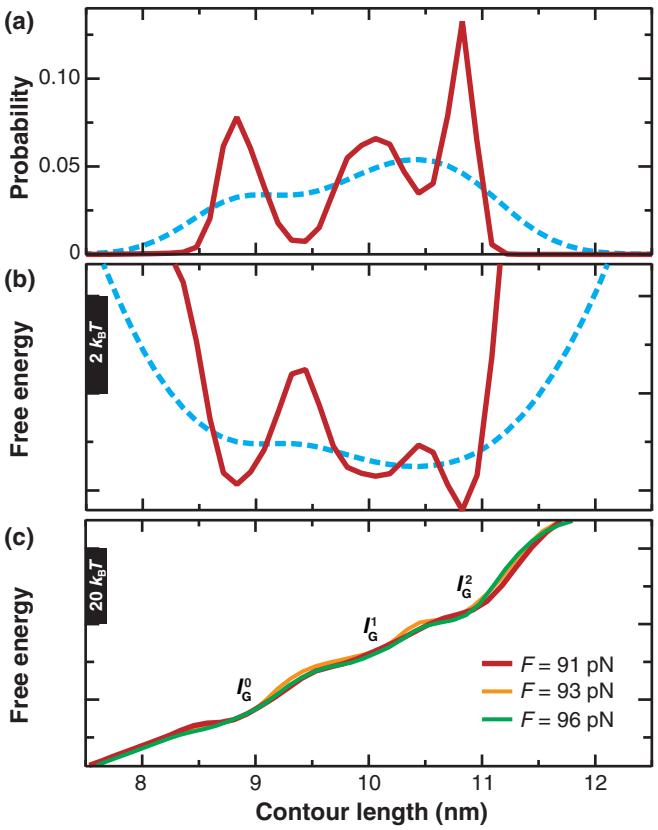

FIG. 4. Reconstruction of the free-energy landscape of the eight-amino-acid region of interest. (a) Probability distribution of extension before (dashed cyan) and after (solid red) deconvolution. (b) Free-energy landscape before (cyan) and after (red) deconvolution. (c) Free-energy landscape at zero applied force recovered from equilibrium trajectories of an individual molecule under three different tensions (91, 93, and 96 pN in state I_G^0). For clarity, extensions are represented as contour lengths of the unfolded polypeptide chain.

separation due to minimal hysteresis, we computed ΔG_0 by simply averaging W over all molecules and velocities to yield $\Delta G_0^{02} = 33.9 \pm 2.2\, k_B T$ [mean ± SEM (10 molecules, 3 velocities, 530 total cycles of unfolding and refolding)]. The CFT is a more general nonequilibrium analysis than the kinetic rate-map strategy because it does not require identifying discrete states. However, here CFT analysis could not separately determine ΔG_0^{01} and ΔG_0^{12} because there was no Z at which state I_G^1 was stably occupied.

Our third method for determining ΔG_0 analyzed equilibrium data [Fig. 1(c)]. We inverted the canonical Boltzmann distribution and accounted for the work done in stretching the protein using

$$\Delta G_0^{ij} = -k_B T \ln\left(\frac{P_j}{P_i}\right) - \Delta G_{\mathrm{cant}} - \Delta G_{\mathrm{linker}} - \Delta G_{\mathrm{released}}, \tag{5}$$

where the P_i are relative occupancies of states [i.e., local maxima in Fig. 4(a)] [58]. The correction terms are the same as in Eq. (3). Applying Eq. (5) to three-state equilibrium records for nine molecules gave $\Delta G_0^{01} = 16.6 \pm 0.6\ k_B T$ (mean ± SEM) for the first transition and $\Delta G_0^{12} = 10.1 \pm 0.6\ k_B T$ for the second, totaling to $\Delta G_0^{02} = 26.8 \pm 0.8\ k_B T$.

The high quality of the data allowed us to go beyond determining ΔG_0 to also reconstruct the full one-dimensional free-energy landscape for select molecules [Fig. 4], similar to pioneering DNA-hairpin [59] and globular-protein [60] studies. To do so, we recorded ~1000 transitions in individual equilibrium trajectories over hundreds of milliseconds. We then recovered the intrinsic molecular landscape by deconvolving the compliance effects of the cantilever and linkers [Fig. 4(a)] [60]. The resulting free-energy landscape showed distinct barriers that were not present prior to deconvolution [Fig. 4(b), red vs cyan]. Finally, we tilted the measured free-energy landscape to zero applied force. We found that the zero-force landscapes for an individual molecule acquired at three different cantilever positions overlapped, lending confidence in the reliability of the deconvolution [Fig. 4(c)]. Moreover, the higher energy barrier of transition $I_G^0 \leftrightarrow I_G^1$ compared to $I_G^1 \leftrightarrow I_G^2$ is

TABLE I. ΔG_0 for the eight-amino-acid transition $I_G^0 \rightarrow I_G^2$ measured by three different methods.

Method	ΔG_0 (k_BT)	ΔG_0 (kcal/mol)
Kinetics	27.7 ± 0.8	16.4 ± 0.5
Crooks fluctuation theorem	33.9 ± 2.2	20.0 ± 1.3
Inverse Boltzmann	26.8 ± 0.8	15.8 ± 0.6

consistent with the slower kinetics for that transition in the rate map of Fig. 2(b). Hence, complementary information from the energy landscape aids in interpreting the rate maps.

The general agreement in ΔG_0 between the three different free-energy analyses (Table I) validates the robustness of each analysis individually and provides a basis for comparison with prior results. Notably, the approaches agreed despite being based on complementary assumptions and utilizing both equilibrium and nonequilibrium data. Application of the Crooks fluctuation theorem was the most challenging; residual noise broadened the work distributions and may have introduced larger uncertainty in determining ΔG_0.

The consensus value of ΔG_0 per amino acid (AA) to unfold the 8-AA region under study was 3.4–4.2 k_BT/AA. Despite our explicitly removing the work to stretch the unfolded peptide, this value was larger than the 0.8–2.2 k_BT/AA of prior AFM measurements that averaged over the final five helices extracted [27–29]. The simplest explanation of our higher value is that it arose from probing the local energetics of initial BR unfolding when all stabilizing tertiary interactions were present. Indeed, prior AFM studies show it is much easier to extract the final 80% of a particular pair of transmembrane helices than to initiate unfolding [29,31,44]. Finally, we note that our value is close to the 4.6 k_BT/AA determined when probing a 3-AA region in the initial unfolding of the ED helix pair of BR [44].

Our ΔG_0 values from force-induced unfolding were ~20-fold larger than those previously measured in chemical-denaturation experiments. This effect is attributable primarily to the very different unfolded states in the two techniques. In particular, force-induced unfolding disrupts both secondary and tertiary structure and transfers most of the unfolded residues from the bilayer into an aqueous environment [Fig. 1(a)]. Thus, our observed ΔG_0 are close to the 22.9 k_BT computed based only on the free-energy change of octanol-water partition (8.0 k_BT [4,61]) and the enthalpic cost of breaking the backbone hydrogen bonds (14.9 k_BT, based on $\Delta H = 1.1$ kcal/mol/AA [62,63], an arguably simplistic assumption [64]). By contrast, the chemically denatured state retains ~60% secondary structure and remains solvated in detergent.

In conclusion, we have demonstrated a force-spectroscopy-based method for measuring the stabilizing energetics of individual membrane proteins in the native lipid bilayer starting from the fully folded state. Importantly, mechanical unfolding of a single molecule avoids the ambiguities of chemical-denaturation experiments (i.e., poorly defined denatured state, detergent interactions). All three of our analyses determined ΔG_0 of the protein's intrinsic, biologically relevant energy landscape by subtracting the energetics associated with the linker and force probe. Each analysis was previously individually validated in nucleic-acid or globular-protein systems [57,59,60]. Now, the general agreement between techniques in membrane-protein studies establishes any of them, separately, as a robust thermodynamic basis for future studies of point-mutant free-energy changes, reconstituted BR in controlled lipid samples, and membrane-protein–ligand interactions.

We thank James Bowie for providing cell lines for making BR mutants, Olga Dudko for helpful discussions, Lyle Uyetake for preparing BR samples, and Devin Edwards for experimental assistance. This work was supported by the National Science Foundation (MCB-1716033; Phy-1734006); the National Institute of Standards and Technology (NIST); and the National Natural Science Foundation of China [Grants No. 11774107 and No. 31971157 (to H. Y.)].

*Corresponding author.
tperkins@jila.colorado.edu
†These authors contributed equally to this work.

[1] F. Cymer, G. von Heijne, and S. H. White, Mechanisms of integral membrane protein insertion and folding, J. Mol. Biol. **427**, 999 (2015).
[2] J. L. Popot, S. E. Gerchman, and D. M. Engelman, Refolding of bacteriorhodopsin in lipid bilayers. A thermodynamically controlled two-stage process, J. Mol. Biol. **198**, 655 (1987).
[3] K. G. Fleming, Energetics of membrane protein folding, Annu. Rev. Biophys. **43**, 233 (2014).
[4] S. H. White and W. C. Wimley, Membrane protein folding and stability: Physical principles, Annu. Rev. Biophys. Biomol. Struct. **28**, 319 (1999).
[5] F. W. Lau and J. U. Bowie, A method for assessing the stability of a membrane protein, Biochemistry **36**, 5884 (1997).
[6] G. Q. Chen and E. Gouaux, Probing the folding and unfolding of wild-type and mutant forms of bacteriorhodopsin in micellar solutions: Evaluation of reversible unfolding conditions, Biochemistry **38**, 15380 (1999).
[7] D. E. Otzen, Folding of DsbB in mixed micelles: A kinetic analysis of the stability of a bacterial membrane protein, J. Mol. Biol. **330**, 641 (2003).
[8] G. H. Huysmans, S. A. Baldwin, D. J. Brockwell, and S. E. Radford, The transition state for folding of an outer membrane protein, Proc. Natl. Acad. Sci. U.S.A. **107**, 4099 (2010).
[9] H. E. Findlay, N. G. Rutherford, P. J. Henderson, and P. J. Booth, Unfolding free energy of a two-domain transmembrane sugar transport protein, Proc. Natl. Acad. Sci. U.S.A. **107**, 18451 (2010).

[10] A. Veerappan, F. Cymer, N. Klein, and D. Schneider, The tetrameric alpha-helical membrane protein GlpF unfolds via a dimeric folding intermediate, Biochemistry **50**, 10223 (2011).

[11] M. R. Sanders, H. E. Findlay, and P. J. Booth, Lipid bilayer composition modulates the unfolding free energy of a knotted alpha-helical membrane protein, Proc. Natl. Acad. Sci. U.S.A. **115**, E1799 (2018).

[12] S. Yohannan, S. Faham, D. Yang, D. Grosfeld, A. K. Chamberlain, and J. U. Bowie, A $C_\alpha - H \ldots O$ hydrogen bond in a membrane protein is not stabilizing, J. Am. Chem. Soc. **126**, 2284 (2004).

[13] S. Yohannan, D. Yang, S. Faham, G. Boulting, J. Whitelegge, and J. U. Bowie, Proline substitutions are not easily accommodated in a membrane protein, J. Mol. Biol. **341**, 1 (2004).

[14] S. Faham, D. Yang, E. Bare, S. Yohannan, J. P. Whitelegge, and J. U. Bowie, Side-chain contributions to membrane protein structure and stability, J. Mol. Biol. **335**, 297 (2004).

[15] N. H. Joh, A. Min, S. Faham, J. P. Whitelegge, D. Yang, V. L. Woods, and J. U. Bowie, Modest stabilization by most hydrogen-bonded side-chain interactions in membrane proteins, Nature (London) **453**, 1266 (2008).

[16] P. Curnow, N. D. Di Bartolo, K. M. Moreton, O. O. Ajoje, N. P. Saggese, and P. J. Booth, Stable folding core in the folding transition state of an alpha-helical integral membrane protein, Proc. Natl. Acad. Sci. U.S.A. **108**, 14133 (2011).

[17] J. P. Schlebach, N. B. Woodall, J. U. Bowie, and C. Park, Bacteriorhodopsin folds through a poorly organized transition state, J. Am. Chem. Soc. **136**, 16574 (2014).

[18] Y. C. Chang and J. U. Bowie, Measuring membrane protein stability under native conditions, Proc. Natl. Acad. Sci. U.S.A. **111**, 219 (2014).

[19] M. L. Riley, B. A. Wallace, S. L. Flitsch, and P. J. Booth, Slow alpha helix formation during folding of a membrane protein, Biochemistry **36**, 192 (1997).

[20] V. Krishnamani, B. G. Hegde, R. Langen, and J. K. Lanyi, Secondary and tertiary structure of bacteriorhodopsin in the SDS denatured state, Biochemistry **51**, 1051 (2012).

[21] H. Hong, N. H. Joh, J. U. Bowie, and L. K. Tamm, Methods for measuring the thermodynamic stability of membrane proteins, Methods Enzymol. **455**, 213 (2009).

[22] J. T. Marinko, H. Huang, W. D. Penn, J. A. Capra, J. P. Schlebach, and C. R. Sanders, Folding and misfolding of human membrane proteins in health and disease: From single molecules to cellular proteostasis, Chem. Rev. **119**, 5537 (2019).

[23] H. K. Choi, D. Min, H. Kang, M. J. Shon, S.-H. Rah, H. C. Kim, H. Jeong, H.-J. Choi, J. U. Bowie, and T.-Y. Yoon, Watching helical membrane proteins fold reveals a common N-to-C-terminal folding pathway, Science **366**, 1150 (2019).

[24] F. Oesterhelt, D. Oesterhelt, M. Pfeiffer, A. Engel, H. E. Gaub, and D. J. Muller, Unfolding pathways of individual bacteriorhodopsins, Science **288**, 143 (2000).

[25] C. A. Bippes and D. J. Muller, High-resolution atomic force microscopy and spectroscopy of native membrane proteins, Rep. Prog. Phys. **74**, 086601 (2011).

[26] M. Zocher, C. A. Bippes, C. Zhang, and D. J. Muller, Single-molecule force spectroscopy of G-protein-coupled receptors, Chem. Soc. Rev. **42**, 7801 (2013).

[27] M. Kessler, K. E. Gottschalk, H. Janovjak, D. J. Muller, and H. E. Gaub, Bacteriorhodopsin folds into the membrane against an external force, J. Mol. Biol. **357**, 644 (2006).

[28] J. Preiner, H. Janovjak, C. Rankl, H. Knaus, D. A. Cisneros, A. Kedrov, F. Kienberger, D. J. Muller, and P. Hinterdorfer, Free energy of membrane protein unfolding derived from single-molecule force measurements, Biophys. J. **93**, 930 (2007).

[29] P. R. Heenan, H. Yu, M. G. W. Siewny, and T. T. Perkins, Improved free-energy landscape reconstruction of bacteriorhodopsin highlights local variations in unfolding energy, J. Chem. Phys. **148**, 123313 (2018).

[30] J. Gore, F. Ritort, and C. Bustamante, Bias and error in estimates of equilibrium free-energy differences from nonequilibrium measurements, Proc. Natl. Acad. Sci. U.S.A. **100**, 12564 (2003).

[31] D. J. Muller, M. Kessler, F. Oesterhelt, C. Moller, D. Oesterhelt, and H. Gaub, Stability of bacteriorhodopsin alpha-helices and loops analyzed by single-molecule force spectroscopy, Biophys. J. **83**, 3578 (2002).

[32] H. Yu, P. R. Heenan, D. T. Edwards, L. Uyetake, and T. T. Perkins, Quantifying the initial unfolding of bacteriorhodopsin reveals retinal stabilization, Angew. Chem. Int. Ed. **58**, 1710 (2019).

[33] D. T. Edwards, J. K. Faulk, A. W. Sanders, M. S. Bull, R. Walder, M. A. LeBlanc, M. C. Sousa, and T. T. Perkins, Optimizing 1-μs-resolution single-molecule force spectroscopy on a commercial atomic force microscope, Nano Lett. **15**, 7091 (2015).

[34] J. K. Faulk, D. T. Edwards, M. S. Bull, and T. T. Perkins, Improved force spectroscopy using focused-ion-beam-modified cantilevers, Methods Enzymol. **582**, 321 (2017).

[35] See Supplemental Material at http://link.aps.org/supplemental/10.1103/PhysRevLett.125.068102 for discussion of experimental procedures, PEG elastic model, and details of the kinetic and inverse-Boltzmann analyses, which includes Refs. [36–38]

[36] P. A. Jansson, *Deconvolution of Images and Spectra*, 2nd ed. (Academic Press, San Diego, 1997).

[37] D. T. Edwards, J. K. Faulk, M. A. LeBlanc, and T. T. Perkins, Force spectroscopy with 9-μs resolution and sub-pN stability by tailoring AFM cantilever geometry, Biophys. J. **113**, 2595 (2017).

[38] F. Rico, L. Gonzalez, I. Casuso, M. Puig-Vidal, and S. Scheuring, High-speed force spectroscopy unfolds titin at the velocity of molecular dynamics simulations, Science **342**, 741 (2013).

[39] R. Walder *et al.*, Rapid characterization of a mechanically labile α-helical protein enabled by efficient site-specific bioconjugation, J. Am. Chem. Soc. **139**, 9867 (2017).

[40] R. Walder, W. J. Van Patten, D. B. Ritchie, R. K. Montange, T. W. Miller, M. T. Woodside, and T. T. Perkins, High-precision single-molecule characterization of the folding of an HIV RNA hairpin by atomic force microscopy, Nano Lett. **18**, 6318 (2018).

[41] J. F. Marko and E. D. Siggia, Stretching DNA, Macromolecules **28**, 8759 (1995).

[42] R. Petrosyan, Improved approximations for some polymer extension models, Rheol. Acta **56**, 21 (2017).
[43] F. Oesterhelt, M. Rief, and H. E. Gaub, Single molecule force spectroscopy by AFM indicates helical structure of poly(ethylene-glycol) in water, New J. Phys. **1**, 6.1 (1999).
[44] H. Yu, M. G. W. Siewny, D. T. Edwards, A. W. Sanders, and T. T. Perkins, Perkins, Hidden dynamics in the unfolding of individual bacteriorhodopsin proteins, Science **355**, 945 (2017).
[45] J. Liphardt, B. Onoa, S. B. Smith, I. J. Tinoco, and C. Bustamante, Reversible unfolding of single RNA molecules by mechanical force, Science **292**, 733 (2001).
[46] G. E. Crooks, Entropy production fluctuation theorem and the nonequilibrium work relation for free energy differences, Phys. Rev. E **60**, 2721 (1999).
[47] Y. J. Zhang and O. K. Dudko, A transformation for the mechanical fingerprints of complex biomolecular interactions, Proc. Natl. Acad. Sci. U.S.A. **110**, 16432 (2013).
[48] L. R. Rabiner, A tutorial on hidden Markov models and selected applications in speech recognition, Proc. IEEE **77**, 257 (1989).
[49] E. Parzen, *Stochastic Processes* (Holden-Day, San Francisco, 1962).
[50] D. R. Jacobson and T. T. Perkins, companion paper, Correcting molecular transition rates measured by single-molecule force spectroscopy for limited temporal resolution, Phys. Rev. E **102**, 022402 (2020).
[51] G. I. Bell, Models for specific adhesion of cells to cells, Science **200**, 618 (1978).
[52] O. K. Dudko, G. Hummer, and A. Szabo, Intrinsic Rates and Activation Free Energies from Single-molecule Pulling Experiments, Phys. Rev. Lett. **96**, 108101 (2006).
[53] I. Tinoco, Jr. and C. Bustamante, The effect of force on thermodynamics and kinetics of single molecule reactions, Biophys. Chem. **101–102**, 513 (2002).
[54] M. T. Woodside, W. M. Behnke-Parks, K. Larizadeh, K. Travers, D. Herschlag, and S. M. Block, Nanomechanical measurements of the sequence-dependent folding landscapes of single nucleic acid hairpins, Proc. Natl. Acad. Sci. U.S.A. **103**, 6190 (2006).
[55] D. R. Jacobson, L. Uyetake, and T. T. Perkins, Membrane-protein unfolding intermediates detected with enhanced precision using a zigzag force ramp, Biophys. J. **118**, 667 (2020).
[56] H. Luecke, B. Schobert, H. T. Richter, J. P. Cartailler, and J. K. Lanyi, Structure of bacteriorhodopsin at 1.55 Å resolution, J. Mol. Biol. **291**, 899 (1999).
[57] D. Collin, F. Ritort, C. Jarzynski, S. B. Smith, I. Tinoco, Jr., and C. Bustamante, Verification of the Crooks fluctuation theorem and recovery of RNA folding free energies, Nature (London) **437**, 231 (2005).
[58] M. T. Woodside and S. M. Block, Reconstructing folding energy landscapes by single-molecule force spectroscopy, Annu. Rev. Biophys. **43**, 19 (2014).
[59] M. T. Woodside, P. C. Anthony, W. M. Behnke-Parks, K. Larizadeh, D. Herschlag, and S. M. Block, Direct measurement of the full, sequence-dependent folding landscape of a nucleic acid, Science **314**, 1001 (2006).
[60] J. C. Gebhardt, T. Bornschlogl, and M. Rief, Full distance-resolved folding energy landscape of one single protein molecule, Proc. Natl. Acad. Sci. U.S.A. **107**, 2013 (2010).
[61] W. C. Wimley, T. P. Creamer, and S. H. White, Solvation energies of amino acid side chains and backbone in a family of host-guest pentapeptides, Biochemistry **35**, 5109 (1996).
[62] J. M. Scholtz, S. Marqusee, R. L. Baldwin, E. J. York, J. M. Stewart, M. Santoro, and D. W. Bolen, Calorimetric determination of the enthalpy change for the alpha-helix to coil transition of an alanine peptide in water, Proc. Natl. Acad. Sci. U.S.A. **88**, 2854 (1991).
[63] T. Ooi and M. Oobatake, Prediction of the thermodynamics of protein unfolding: The helix-coil transition of poly(L-alanine), Proc. Natl. Acad. Sci. U.S.A. **88**, 2859 (1991).
[64] Z. Cao, J. M. Hutchison, C. R. Sanders, and J. U. Bowie, Backbone hydrogen bond strengths can vary widely in transmembrane helices, J. Am. Chem. Soc. **139**, 10742 (2017).